Applied Materials Today 20 (2020) 100668

Contents lists available at ScienceDirect

Applied Materials Today

journal homepage: www.elsevier.com/locate/apmt

Jahn–Teller distortion-driven robust blue-light-emitting perovskite nanoplatelets

G. Krishnamurthy Grandhi[a], H.C. Manas Likhit[b], Shyue Ping Ong[b,*], Won Bin Im[a,*]

[a] Division of Materials Science and Engineering, Hanyang University, 222 Wangsimni-ro, Seongdong-gu, Seoul 04763, Republic of Korea
[b] Department of Nanoengineering, University of California, San Diego, CA 92093, United States

ARTICLE INFO

Article history:
Received 9 December 2019
Revised 4 April 2020
Accepted 14 April 2020

Keywords:
$CsPbBr_3$ nanoplatelets
Blue emission
Cu^{2+} doping
Jahn–Teller distortion
Surface energy

ABSTRACT

Blue-light-emitting and quantum-confined two-dimensional $CsPbBr_3$ perovskite nanoplatelets (NPLs) are viable candidates for blue-light-emitting diodes compared to mixed-halide $CsPb(Br/Cl)_3$ nanocrystals that exhibit segregation of halide ions. Unfortunately, the NPLs suffer from poor color stability and insufficient colloidal stability. However, the improvement in their stability has not been extensively studied. In this study, the blue emission of $CsPbBr_3$ NPLs is stabilized by B-site doping approach, wherein a few of Pb^{2+} octahedral sites are replaced with small-sized Cu^{2+} ions. Cu^{2+}-doped NPLs exhibit greater long-term stability in ambient conditions and better photostability compared to their undoped counterparts. First-principles calculations reveal that the Jahn–Teller distortion of $(CuBr_6)^{4-}$ octahedra results in the shorter Pb-Br bonds and contraction of the entire $CsPbBr_3$ lattice, which in turn increases the band gap of the $CsPbBr_3$ NPLs. Cu^{2+} dopants also reduce the surface energy of the NPLs and impart highly desirable long-term stability. Therefore, the outcomes of this work might be a step forward towards improving the stability of two-dimensional perovskite NPLs.

1. Introduction

The application of three-dimensional (3D) cesium lead halide perovskite nanocrystals (NCs) in light-emitting diodes (LEDs) has been on the rise in recent years [1–4]. Their emission colors change from blue to near-infrared as the halide varies from chloride to bromide to iodide [5]. Green and red emissions can be obtained from bromide- and iodide-based NCs, respectively, while blue-light-emitting NCs have predominantly been produced by mixing bromides and chlorides. Although highly efficient green- [1,3] and red-light-emitting [2,6] perovskite LEDs have been successfully fabricated, mixed-halide-based blue-light-emitting perovskite LEDs exhibit color instability owing to the segregation of the halide ions, which in turn leads to shifts in the emission wavelengths during LED operation [7,8]. Moreover, blue perovskite LEDs trail behind the green and red perovskite LEDs in stability and efficiency [9]. Blue emitters with wavelengths of ~465–475 nm are required according to National Television System Committee (NTSC) standards and International Telecommunication Union Radiocommunication Sector (ITU-R) standards for display applications [10,11]. Blue light emission can arise even from $CsPbBr_3$ NCs when their size is smaller than the exciton Bohr radius. They are usually obtained as nanoplatelets (NPLs), which are quantum-confined two-dimensional (2D) nanostructures [12,13]. The band gap of the NPLs strongly depends upon their thickness; a lower thickness results in a higher band gap. Nonetheless, NPLs based on lead halides also suffer from low photoluminescence (PL) efficiency and poor colloidal and emission stabilities. Recently, their PL efficiencies were improved through post-synthesis surface repair or in situ surface passivation [12,14]; however, their long-term stability has not been addressed in detail thus far. For instance, the emission wavelengths of $CsPbBr_3$ NPLs shift to higher wavelengths within a few hours after synthesis and the NPLs lose their colloidal stability, owing to the fusion or self-assembly of small NPLs into larger green-emitting NCs [15]. It may be attributed to the increase in the surface energy of the NPLs upon their thicknesses being reduced [16]. Only limited efforts have been established to address the stability issues of perovskite NPLs [12]. Therefore, a simple and efficient strategy to stabilize the blue emission of $CsPbBr_3$ NPLs, which is essential for their application in optoelectronic devices, is necessary.

B-site doping approach has been utilized for improving the stability of $CsPbX_3$-type (X = Cl, Br, I) perovskite materials, wherein a small portion of the B-site ions is substituted with various isovalent ions [17]. The stabilization usually arises from a slightly contracted host lattice and, hence, a small increase in its tolerance

* Corresponding author.
E-mail addresses: ongsp@eng.ucsd.edu (S.P. Ong), imwonbin@hanyang.ac.kr (W.B. Im).

https://doi.org/10.1016/j.apmt.2020.100668
2352-9407/

factor. Small-sized dopants such as Bi^{3+}, Mn^{2+}, Ni^{2+} Cu^{2+}were explored to improve phase stability, PL efficiency and chemical stability of $CsPbX_3$ NCs and thin films [18–21] Furthermore, Mn^{2+}ions were successfully incorporated into 2D $CsPbCl_3$ NPLs and their optical properties were studied. [22] Nonetheless, B-site doping approach has not been employed for stabilizing perovskite NPLs.

In this study, B-site doping approach was exploited for obtaining stable 2D perovskites. We chose Cu^{2+}ions as dopants and $CsPbBr_3$ NPLs as the host for this study and found that the long-term stability of blue-light-emitting $CsPbBr_3$ NPLs are improved upon the Cu^{2+}doping. The origin of dopant-induced stability was discussed with the help of computational and experimental studies.

2. Experimental section

2.1. Materials

All reagents were used without any further purification: cesium carbonate (Cs_2CO_3, 99.999%, Kojundo), lead(II) bromide ($PbBr_2$, 99%, Sigma-Aldrich), copper bromide ($CuBr_2$, Sigma-Aldrich), oleic acid (OlAc, 90%, Fluka), oleylamine (OlAm, Sigma-Aldrich), 1-octadecene (ODE, 95%, Sigma-Aldrich), toluene (99.8%, Junsei), and *n*-hexane (99.8%, Junsei).

2.2. Synthesis of precursors

A pale yellow cesium oleate precursor was obtained by dissolving 0.1 mmol of Cs_2CO_3 in 10 mL of oleic acid at 100 °C under continuous stirring. The $PbBr_2$ precursor solution was prepared by heating 0.1 mmol of $PbBr_2$ powder and 100 μL each of OlAc and OlAm in 10 mL of toluene at above 100 °C until all of the $PbBr_2$ had dissolved.

2.3. Synthesis of undoped and Cu^{2+}-doped $CsPbBr_3$NPLs

The synthesis of the NPLs was performed at room temperature and under an ambient environment. Cesium oleate (150 µL) precursor was injected into a toluene solution containing the $PbBr_2$–OlAm/OlAc precursor (1.5 mL) under vigorous stirring. Acetone (2 mL) was added after 5 s to initiate the nucleation of the NPLs. After 1 min of stirring, the solution was centrifuged at 4000 rpm for 3 min and the so-obtained precipitate was redispersed in hexane (1–2 mL) for further studies. For the synthesis of Cu^{2+}-doped NPLs, a mixture of $PbBr_2$ and $CuBr_2$ was used.

2.4. Characterization and spectroscopic techniques

Structure and size determination for the NCs were carried out using X-ray diffraction (XRD) and transmission electron microscopy (TEM). XRD was performed on thin films of the synthesized NCs, and patterns were recorded on a Shimadzu X-ray diffractometer using Cu K_α radiation. All patterns were recorded at a low rate of 1° per minute to obtain a high signal-to-noise ratio. The Visualization for Electronic and Structural Analysis (VESTA) program was used to draw the crystal structures. [23] Low- and high-resolution TEM images were recorded using an FEI Tecnai F20 (200 kV), at the Korea Basic Science Institute (KBSI), Gwangju, South Korea. The samples for the TEM measurements were prepared by dispersing the NCs in *n*-hexane. It is worth mentioning that cesium lead bromide NCs are usually not stable under irradiation with high-energy electron beams and tend to decompose within a short time. The chemical compositions of the synthesized NPLs were analyzed using ICP-OES (PerkinElmer, OPTIMA 8300) at the Korea Basic Science Institute (KBSI), Gwangju, South Korea. EPR measurements were carried out using a JEOL JES-FA200 with an X-band microwave frequency of 9.17 GHz, with NPL dispersions in hexane at 173 K and at room temperature. The liquid samples were transferred to EPR tubes and frozen in liquid nitrogen at 173 K. All spectra were recorded using the following EPR parameters: microwave power, 1 mW; modulation amplitude, 0.2 mT; modulation frequency, 100 kHz; and sweep time, 120 s. UV–visible absorption spectra of various aliquots dissolved in hexane were obtained using a Thermo Scientific Evolution 201 UV-visible spectrometer. Steady-state PL spectra in *n*-hexane were collected using a Hitachi F-4500 fluorescence spectrophotometer.

The complete details of the first principle calculations of the bandgap and surface energy calculations using density functional theory (DFT) are given in Computational details section in the Supporting information (SI).

3. Results and discussion

Table S1 of the SI shows the Goldschmidt tolerance factor for Cu^{2+}-doped $CsPbBr_3$ as a function of Cu^{2+} concentration. The tolerance factor increased gradually towards a value of 1 with increasing amount of Cu^{2+}, suggesting that Cu^{2+} doping can stabilize the cubic phase of $CsPbBr_3$. In this study, both undoped and Cu^{2+}-doped $CsPbBr_3$ NPLs were synthesized using a reprecipitation method, [12] wherein cesium oleate was introduced into a mixture of $PbBr_2$ and $CuBr_2$ (step I) and then a polar solvent was added to initiate the nucleation of the NPLs (step II), as shown in Fig. 1a. Inductively coupled plasma optical emission spectroscopy (ICP-OES) was employed to confirm the incorporation of Cu^{2+} ions into the $CsPbBr_3$ lattice, as shown in Table S2 of the SI. Fig. 1b and 1c show the TEM images of the undoped and Cu^{2+}-doped NPLs. Fig. 1c suggests that the Cu^{2+}-doped NPLs formed with a uniform size distribution. The thicknesses of both the undoped and Cu^{2+}-doped NPLs were ~2–3 nm, indicating that they are only a few monolayers thick. The formation of the NPLs was also confirmed by XRD studies, as shown in Figure S1 of the SI. The XRD patterns mainly show the 001 and 002 planes of cubic-phase $CsPbBr_3$, suggesting the preferential orientation of the 2D NPLs on the substrate. The XRD peaks for the Cu^{2+}-doped NPLs were shifted slightly towards higher angles, further suggesting the successful incorporation of small-sized Cu^{2+} ions into the $CsPbBr_3$ lattice. Fig. 1d shows the X-band electron paramagnetic resonance (EPR) spectrum of Cu^{2+}-doped $CsPbBr_3$ NPLs, collected at a low temperature in *n*-hexane. The spectrum shows a broad signal centered at ~325 mT, suggesting that the Cu^{2+} dopants exist in the paramagnetic +2 oxidation state (d^9 system). The Lande factor (g-factor) calculated from the EPR spectrum was approximately 2.08, suggesting that Cu^{2+} ions occupy the octahedral [24] (Pb^{2+}) sites of $CsPbBr_3$, as shown in Fig. 1e. Fig. 1f and g show the ultraviolet (UV)-visible absorption spectra and PL spectra of undoped and Cu^{2+}-doped NPLs, respectively. The PL maxima of both types of NPLs are at ~460 nm, corresponding to $CsPbBr_3$ NPLs that are three monolayers thick [12]. Furthermore, there was a small blue shift in both the absorption and PL spectra of the $CsPbBr_3$ NPLs upon the incorporation of Cu^{2+}, and the origin of this shift will be discussed in a subsequent section. The PL QY of undoped NPLs was 15–20%. It is to be noted that the PL efficiency of the $CsPbBr_3$ NPLs before and after doping with 5–10% Cu^{2+} was similar, and is quenched when doped with >10% Cu^{2+}. This suggests that Cu-doping has not affected the host optical properties. Furthermore, the absence of secondary emission peaks in the PL and absorption spectra suggests that larger $CsPbBr_3$ nanocubes were not obtained as impurities during NPL synthesis.

Colloidal dispersions of undoped NPLs stored in the ambient atmosphere and under room light witnessed a gradual shift in their emission maximum towards higher wavelengths until green-emitting NCs were produced, as shown in Fig. 2a. This may be attributed to the fusion of the $CsPbBr_3$ NPLs into larger NCs [15,25].

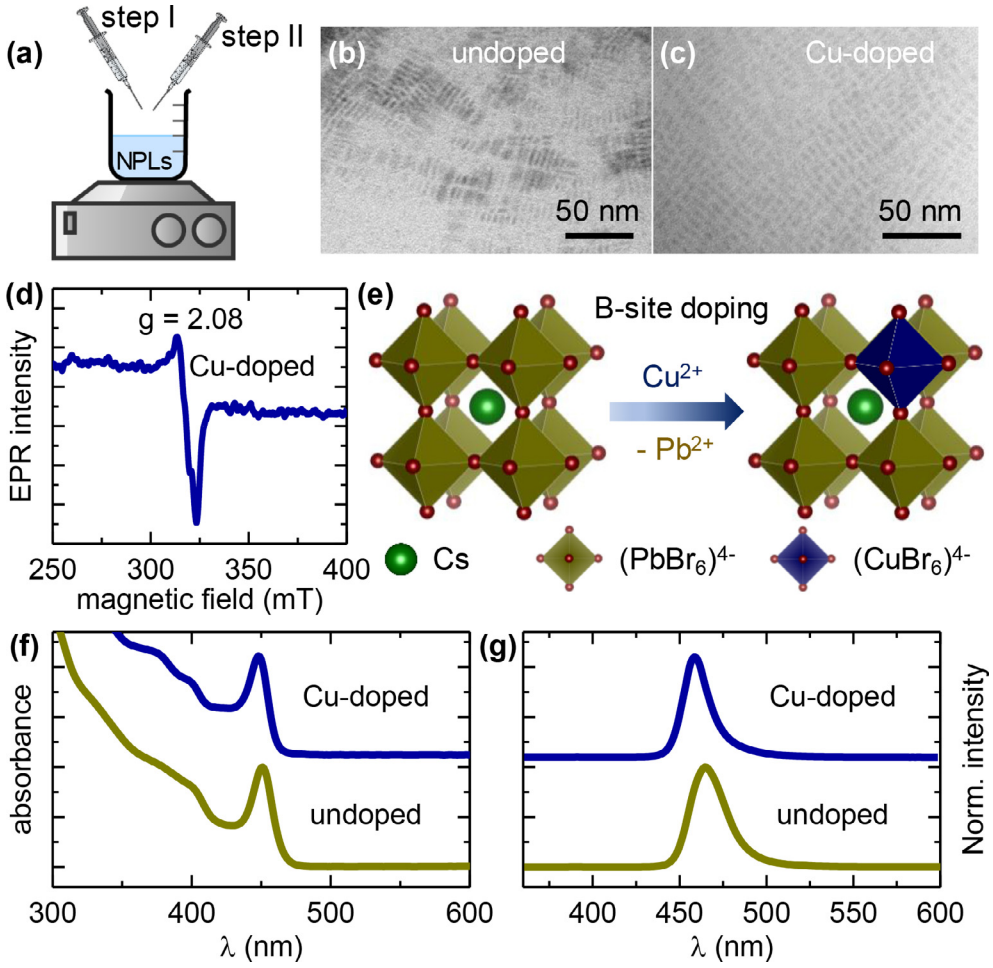

Fig. 1. Characterization of undoped and Cu^{2+}-doped $CsPbBr_3$ NPLs. (a) Schematic representation of NPL synthesis: mixing of capping ligands with Cs, Pb, and Cu precursors (step I), followed by addition of acetone (step II). TEM images of (b) undoped and (c) Cu^{2+}-doped NPLs. (d) EPR spectrum of Cu^{2+}-doped NPLs. (e) Illustration of Cu^{2+} incorporation into the $CsPbBr_3$ lattice. (f) Absorption and (g) PL spectra of the NPLs. λ_{ex} = 350 nm.

On the other hand, a little Cu^{2+} incorporation preserved the blue emission of $CsPbBr_3$ NPLs when stored in the same conditions. Fig. 2b shows that the PL maximum of undoped NPLs shifted gradually from 460 nm to 520 nm within 15 days and that these NPLs lost their colloidal stability. In the case of Cu^{2+}-doped ones, the emission position shifted by <5 nm even after a month of storage in air and their colloidal stability was retained. Nearly 70% of the original PL efficiency was retained for the Cu^{2+}-doped NPLs while the emission position was preserved when they were stored for more than a week in air, as shown in Figure S2 of the SI. This implies that Cu^{2+} incorporation dramatically improves the stability of $CsPbBr_3$ NPLs. Cu^{2+} doping also affected the photostability of the NPLs. Fig. 2c shows the PL of both undoped and Cu^{2+}-doped $CsPbBr_3$ NPLs as a function of UV light exposure time. In the case of undoped NPLs, the PL intensity decreased and the PL maximum gradually red-shifted upon exposure to UV radiation. On the other hand, Cu^{2+}-doped NPLs retained their emission peak position and shape and ~50% of the original PL intensity upon exposure to UV radiation for 6 h, as shown in Fig. 2c. The variations in the PL maximum wavelength as a function of UV irradiation time are presented in Fig. 2d. Notably, in both cases, Cu^{2+}-doped NPLs successfully retained their colloidal stability, while their undoped counterparts failed to do so. Therefore, Cu^{2+} doping dramatically enhances the colloidal stability of the NPLs. Figure S3 of the SI shows photographs of both the undoped and Cu^{2+}-doped NPLs stored in hexane and protected from light at various times. The undoped NPLs gradually lost their colloidal stability, while the Cu^{2+}-doped ones remained colloidally stable for weeks.

The UV-visible absorption band of the $CsPbBr_3$ NPLs was blue-shifted upon Cu^{2+} doping (Fig. 1c), suggesting an increase in the band gap of the NPLs. The conduction band (CB) and valence band (VB) of lead bromide perovskite NCs are composed of Pb 6p orbitals and Br 4p orbitals, respectively. The increase in the band gap may be attributed to the stronger interaction of metal and halide orbitals. To verify this, the band structures of undoped and Cu^{2+}-doped $CsPbBr_3$ were obtained using DFT calculations with the generalized gradient approximation (GGA) functional, as shown in Fig. 3a and b. The calculated bandgap increased from 1.76 eV for undoped $CsPbBr_3$ to 1.87 eV for 5% and 1.88 eV for 10% Cu^{2+} doping respectively. This qualitative trend is consistent with the observed blue shifting of the absorption spectra with the Cu doping, though the GGA band gaps are significantly underestimated as expected. For relaxed structures (see Table S3-S5 of the SI), we find the Pb-Br bond lengths (~3.00 Å) and Br-Pb-Br bond angles (90°) are same for all the $(PbBr_6)^{4-}$ octahedra in case of undoped $CsPbBr_3$ (Fig. 3c). In the case of 5% Cu^{2+}-doped $CsPbBr_3$, the equatorial Cu-Br bonds (along a and b axis) are shorter (2.59 Å) than the axial ones (2.96 Å) of $(CuBr_6)^{4-}$ octahedra (Fig. 3d), suggesting Jahn–Teller distortion; and the difference in the bond lengths becomes more prominent with further increase in the amount of Cu^{2+} in the system, as shown in Table S5 of SI. Additionally, the shortening of a few Pb-Br bonds (2.59 Å and 2.96 Å) results in

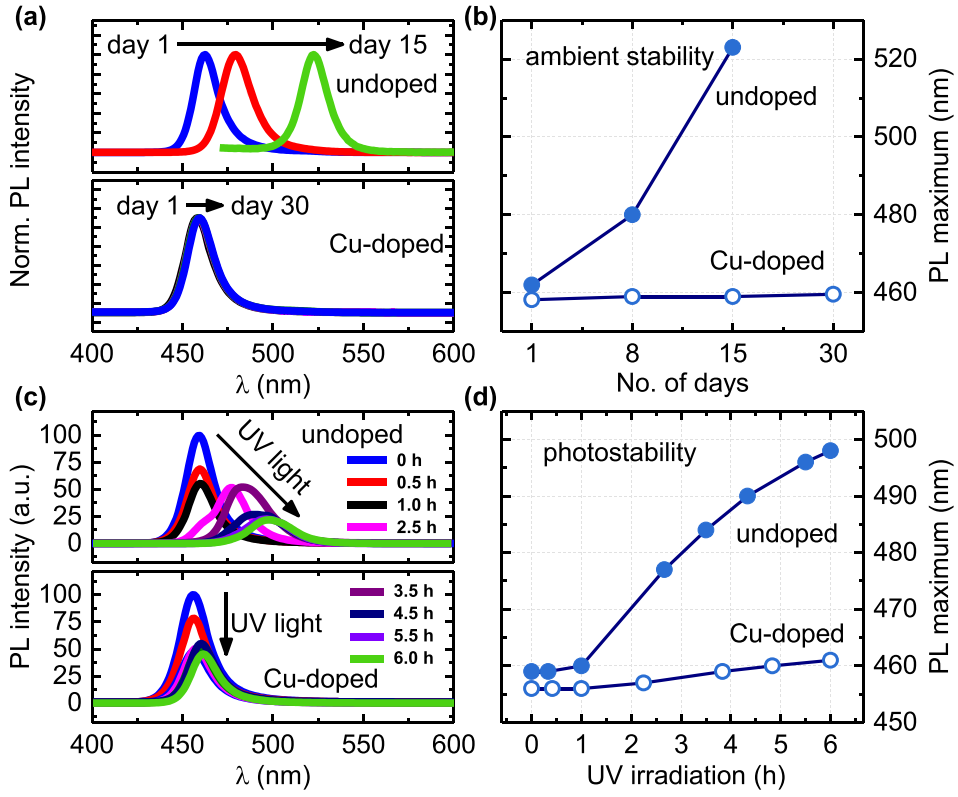

Fig. 2. Long-term and photo stabilities of NPLs. (a) Normalized PL spectra of undoped (top) and Cu^{2+}-doped (bottom) NPLs as a function of time stored in ambient conditions and (b) their corresponding PL maximum wavelengths. (c) PL spectra of undoped (top) and Cu^{2+}-doped (bottom) NPLs as a function of UV irradiation time and (d) their corresponding PL maximum wavelengths.

slight contraction in the a and b lattice parameters of about 0.5% with 5% Cu^{2+}doping, consistent with the observed shift in the XRD peaks (see Figure S1 and Table S6 of the SI). The shortening of Pb-Br bonds in the $CsPbBr_3$ lattice upon doping with small-sized cations has also been observed earlier. [26] Therefore, the shortening of Cu-Br bonds due to Jahn–Teller distortion may have eventually resulted in the contraction of the entire host lattice. The shortening of the Cu-Br bonds due to Jahn–Teller compression (Fig. 3e) and the subsequent lattice contraction would have strengthened the $CsPbBr_3$ lattice. Furthermore, the surface-to-volume ratio of the 2D NPLs is very high compared to that of 3D green-emitting $CsPbBr_3$ NCs. Consequently, the surface portion of the NPLs is expected to play a significant role in determining the stability of the NPLs.

According to the outcomes of the stability experiments (Fig. 2), $CsPbBr_3$ NPLs were initially transformed into cyan-emitting NCs and then converted into green-emitting cubic $CsPbBr_3$ NCs under either room light or UV radiation. This suggests a gradual transformation of 2D NPLs into 3D NCs through the self-assembly or fusion in order to reduce their high surface energy, as shown in Fig. 3f. On the other hand, Cu^{2+} dopants stabilized the blue emission of the NPLs exposed to the ambient atmosphere or UV light, as shown in Fig. 3g. This suggests that Cu^{2+}doping may have reduced the surface energy of the NPLs and preserved their emission characteristics.

DFT calculations were performed to test if Cu^{2+} doping lowers the surface energy of $CsPbBr_3$. From Fig. 4a, it can be observed that the CsBr-terminated (100) surface was found to have higher thermodynamic stability (means lower grand thermodynamic potential F) than the $PbBr_2$-terminated surface for the entire range of μ_{PbBr_2}. Hence, the CsBr-terminated surface was used to analyze the effect of Cu^{2+} doping on the surface energy. Fig. 4b and c show the energy difference between the surfaces of Cu^{2+}-doped and undoped $CsPbBr_3$ within the chemical potential ranges for which $CsPbBr_3$ is stable against the formation of $CsCuBr_3$, CsBr, and $PbBr_2$. In general, it was observed that Cu^{2+} doping leads to a reduction in surface energy of $CsPbBr_3$, with a larger decrease (−30 to −36 mJ/m^2) observed for a higher doping percentage of 12.5%. Fig. 4d and e show the relaxed structures obtained from the DFT calculations for undoped and 6.25% Cu^{2+}-doped slabs, respectively. The misalignment of Pb-Br bonds near the surface of Cu^{2+}-doped $CsPbBr_3$ suggests an increase in lead bromide octahedral rotation near the surface. This effect is more pronounced in the case of 12.5% Cu^{2+}-doped $CsPbBr_3$.Octahedral rotation in perovskites has been very well studied and is known to decrease the total energy of the structure. [27–30] So, the lead bromide octahedral rotation observed near the surface of Cu^{2+}-doped $CsPbBr_3$ might be one of the reasons for the lowering of its surface energy. These calculations are consistent with the experimental outcomes.

This is in line with an earlier demonstration that the surface chemistry of $CsPbBr_3$ NPLs plays a significant role in stabilizing their emission characteristics [12]. Furthermore, Mn^{2+} dopants stabilized the black phase of $CsPbI_3$ NCs by altering the surface energy of the host [31]. On the whole, our strategy of Cu^{2+} doping provides much-needed stability to blue-light-emitting perovskite NPLs, and the addition of $PbBr_2$ known to enhance their PL efficiency; therefore, a combination of Cu^{2+} doping and NPL surface passivation produces NPLs with better stability and high PL efficiency (see SI Figure S4), which are desired characteristics for practical device applications. Furthermore, since Cu exists in the +2 oxidation state, the system can undergo non-linear Zeeman effects [32,33]. Computational calculations (Fig. 3b) also show that Cu^{2+}-doped $CsPbBr_3$ exhibits a net magnetic moment (up spin in blue

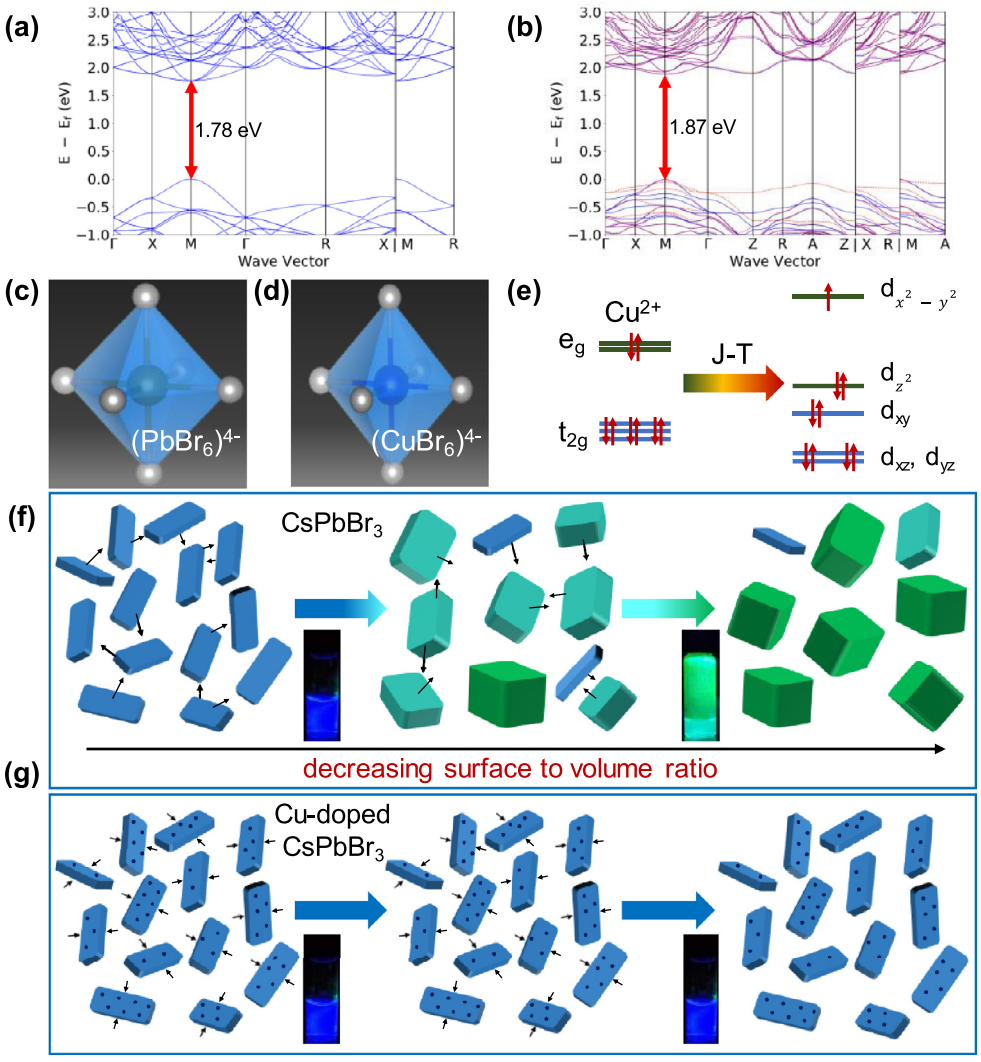

Fig. 3. Jahn–Teller distortion in Cu^{2+} doped NPLs. The density of states of (a) undoped and (b) 5% Cu^{2+}-doped $CsPbBr_3$. Illustrations of (c) $(PbBr_6)^{4-}$ in undoped $CsPbBr_3$ and (d) $(CuBr_6)^{4-}$ octahedra in Cu^{2+}-doped $CsPbBr_3$. The contraction of the four equatorial bonds in $(CuBr_6)^{4-}$ octahedra indicates the Jahn–Teller effect. gray, green, and blue spheres represent Br, Pb, and Cu, respectively. (e) The splitting of t_{2g} and e_g energy levels of Cu^{2+} ions due to Jahn–Teller distortion in the octahedral geometry. Schematics representing the long-term stability of (f) undoped and (g) Cu^{2+}-doped NPLs in the ambient atmosphere or under UV radiation. The images of the vials in the insets of (f) and (g) show the variations in NPL emission as a function of storage time in the ambient atmosphere. (For interpretation of the references to color in this figure legend, the reader is referred to the web version of this article.)

and down spin in red). Therefore, this system can be examined for potential applications in magneto-optical storage [32].

4. Conclusions

The B-site doping has been shown to improve phase stability, chemical stability, and PL QY of 3D perovskite NCs [17,18,20]; however, it is applied to 2D perovskite NPLs here for the first time. Cu^{2+}-doped $CsPbBr_3$ NPLs were synthesized using a modified reprecipitation method. ICP and EPR studies confirmed that Cu dopants exist in the +2 oxidation state and enter the octahedral crystal sites of $CsPbBr_3$. Computational studies showed that Cu^{2+} doping widens the band gap of $CsPbBr_3$ and $(CuBr_6)^{4-}$ octahedra undergo Jahn–Teller distortion, resulting in the contraction and stabilization of the $CsPbBr_3$ lattice. The Cu^{2+}-doped NPLs exhibited long-term color stability in the ambient atmosphere and under UV light and displayed good colloidal stability. The DFT calculations further demonstrated that Cu^{2+} doping reduces the surface energy of the host NPLs, and hence, they retained their structure and emission properties. Future research may involve the utilization of Cu^{2+} doping strategy for fabricating stable blue-light-emitting diodes and studying Cu^{2+}-doped NPLs using magneto-optical spectroscopy.

Supporting information

XRD patterns of undoped and Cu-doped NPLs, PL data for long-term stability of NPLs, colloidal stability study of NPLs, effect of NPL surface passivation, and structure optimization and surface energy results.

Declaration of Competing Interest

The authors declare that they have no known competing financial interests or personal relationships that could have appeared to influence the work reported in this paper.

CRediT authorship contribution statement

G. Krishnamurthy Grandhi: Conceptualization, Resources, Validation, Investigation. **H.C. Manas Likhit:** Conceptualization, Soft-

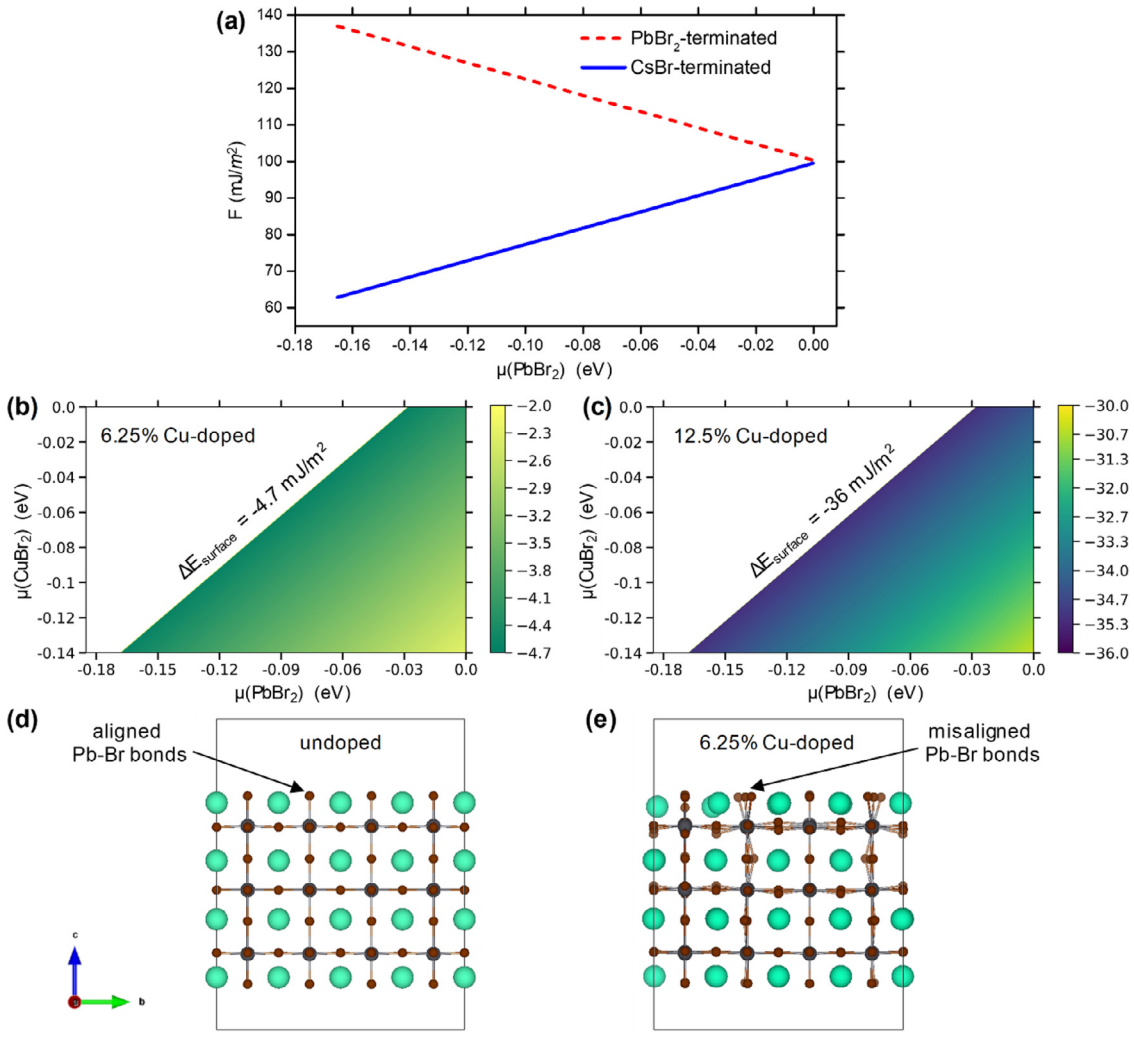

Fig. 4. Origin of NPL stability via Cu^{2+} doping. (a) The grand thermodynamic potential F of the cubic phase of $CsPbBr_3$ as a function of μ_{PbBr_2} for the two types of surface terminations. Contour plot for the difference in surface energies of the doped and undoped $CsPbBr_3$ in case of (b) 6.25% and (c) 12.5% Cu^{2+} doping within the chemical potential bounds. These dopant concentrations are close to those used in the experiments. (d) Undoped and (e) 6.25% Cu^{2+}-doped $CsPbBr_3$ slab structures obtained from DFT calculations (gray: Pb; Brown: Br; Cyan: Cs). (For interpretation of the references to color in this figure legend, the reader is referred to the web version of this article.)

ware. **Shyue Ping Ong:** Conceptualization, Writing - review & editing. **Won Bin Im:** Conceptualization, Writing - review & editing.

Acknowledgements

This research was supported by the Basic Science Research Program through the National Research Foundation of Korea (NRF), funded by the Ministry of Science, ICT & Future Planning (project no. 2017R1A2B3011967). This work was also supported by the Engineering Research Center through the NRF, funded by the Korean Government (MSIT) (project no. NRF-2018R1A5A1025224). This work was also supported by the Technology Innovation Program (KEIT-20002947) funded by the Ministry of Trade, Industry & Energy (MOTIE, Korea).

Supplementary materials

Supplementary material associated with this article can be found, in the online version, at doi:10.1016/j.apmt.2020.100668.

References

[1] K. Lin, J. Xing, L.N. Quan, F.P.G. de Arquer, X. Gong, J. Lu, et al., Perovskite light-emitting diodes with external quantum efficiency exceeding 20 per cent, Nature 562 (2018) 245.
[2] N. Wang, L. Cheng, R. Ge, S. Zhang, Y. Miao, W. Zou, et al., Perovskite light-emitting diodes based on solution-processed self-organized multiple quantum wells, Nat. Photonics 10 (2016) 699.
[3] J. Song, J. Li, L. Xu, J. Li, F. Zhang, B. Han, et al., Room-Temperature Triple-Ligand Surface Engineering Synergistically Boosts Ink Stability, Recombination Dynamics, and Charge Injection toward EQE-11.6% Perovskite QLEDs, Adv. Mater. 30 (2018) 245.
[4] X. Zhang, C. Sun, Y. Zhang, H. Wu, C. Ji, Y. Chuai, et al., Bright perovskite nanocrystal films for efficient light-emitting devices, J. Phys. Chem. Lett. 7 (2016) 4602.
[5] L. Protesescu, S. Yakunin, M.I. Bodnarchuk, F. Krieg, R. Caputo, C.H. Hendon, et al., Nanocrystals of cesium lead halide perovskites ($CsPbX_3$, X= Cl, Br, and I): novel optoelectronic materials showing bright emission with wide color gamut, Nano lett. 15 (2015) 3692.
[6] J. Pan, Y. Shang, J. Yin, M. De Bastiani, W. Peng, I. Dursun, et al., Bidentate ligand-passivated $CsPbI_3$ perovskite nanocrystals for stable near-unity photoluminescence quantum yield and efficient red light-emitting diodes, J. Am. Chem. Soc. 140 (2017) 562.
[7] X. Zhao, J.D.A. Ng, R.H. Friend, Z.-K. Tan, Opportunities and challenges in perovskite light-emitting devices, ACS Photonics 5 (2018) 3866.
[8] S.J. Yoon, M. Kuno, P.V. Kamat, Shift happens. How halide ion defects influence photoinduced segregation in mixed halide perovskites, ACS Energy Lett. 2 (2017) 1507.
[9] C.-H.A. Li, Z. Zhou, P. Vashishtha, J.E. Halpert, The Future Is Blue (LEDs): Why Chemistry Is the Key to Perovskite Displays §, Chem. Mater. 31 (2019) 6003.
[10] K. Masaoka, Y. Nishida, M. Sugawara, Designing display primaries with currently available light sources for UHDTV wide-gamut system colorimetry, Opt. Express 22 (2014) 19069.
[11] S. Hou, M.K. Gangishetty, Q. Quan, D.N. Congreve, Efficient blue and white perovskite light-emitting diodes via manganese doping, Joule 2 (2018) 2421.

[12] B.J. Bohn, Y. Tong, M. Gramlich, M.L. Lai, M. Döblinger, K. Wang, et al., Boosting tunable blue luminescence of halide perovskite nanoplatelets through postsynthetic surface trap repair, Nano lett. 18 (2018) 5231.
[13] Y. Bekenstein, B.A. Koscher, S.W. Eaton, P. Yang, A.P. Alivisatos, Highly luminescent colloidal nanoplates of perovskite cesium lead halide and their oriented assemblies, J. Am. Chem. Soc. 137 (2015) 16008.
[14] Y. Wu, C. Wei, X. Li, Y. Li, S. Qiu, W. Shen, et al., In Situ Passivation of PbBr64-Octahedra toward Blue Luminescent CsPbBr3 Nanoplatelets with Near 100% Absolute Quantum Yield, ACS Energy Lett. 3 (2018) 2030.
[15] V.K. Ravi, A. Swarnkar, R. Chakraborty, A. Nag, Excellent green but less impressive blue luminescence from CsPbBr3 perovskite nanocubes and nanoplatelets, Nanotechnology 27 (2016) 325708.
[16] Y. Yang, F. Gao, S. Gao, M. Sugawara, S.-H. Wei, Origin of the stability of two-dimensional perovskites: a first-principles study, J. Mater. Chem. A 6 (2018) 14949.
[17] A. Swarnkar, W.J. Mir, A. Nag, Can B-site doping or alloying improve thermal-and phase-stability of all-inorganic $CsPbX_3$ (X= Cl, Br, I) perovskites? ACS Energy Lett. 3 (2018) 286.
[18] Q.A. Akkerman, D. Meggiolaro, Z. Dang, F. De Angelis, L. Manna, Fluorescent Alloy $CsPb_xMn_{1-x}I_3$ Perovskite Nanocrystals with High Structural and Optical Stability, ACS Energy Lett. 2 (2017) 2183.
[19] Z.-J. Yong, S.-Q. Guo, J.-P. Ma, J.-Y. Zhang, Z.-Y. Li, Y.-M. Chen, et al., Doping-enhanced short-range order of perovskite nanocrystals for near-unity violet luminescence quantum yield, J. Am. Chem. Soc. 140 (2018) 9942.
[20] C. Bi, S. Wang, Q. Li, S.V. Kershaw, J. Tian, A.L. Rogach, Thermally Stable Copper (II)-Doped Cesium Lead Halide Perovskite Quantum Dots with Strong Blue Emission, J. Phys. Chem. Lett. 10 (2019) 943.
[21] Y. Hu, F. Bai, X. Liu, Q. Ji, X. Miao, T. Qiu, et al., Bismuth incorporation stabilized α-CsPbI3 for fully inorganic perovskite solar cells, ACS Energy Lett. 2 (2017) 2219.
[22] W.J. Mir, M. Jagadeeswararao, S. Das, A. Nag, et al., Colloidal Mn-doped cesium lead halide perovskite nanoplatelets, ACS Energy Lett. 2 (2017) 537.
[23] K. Momma, F. Izumi, VESTA: a three-dimensional visualization system for electronic and structural analysis, J. Appl. Crystallogr. 41 (2008) 653.
[24] N. Singhal, R. Chakraborty, P. Ghosh, A. Nag, et al., Low-Bandgap $Cs_4CuSb_2Cl_{12}$ Layered Double Perovskite: Synthesis, Reversible Thermal Changes, and Magnetic Interaction, Chem. Asian J. 13 (2018) 2085.
[25] Q.A. Akkerman, S.G. Motti, A.R. Srimath Kandada, E. Mosconi, V. D'Innocenzo, G. Bertoni, et al., Solution synthesis approach to colloidal cesium lead halide perovskite nanoplatelets with monolayer-level thickness control, J. Am. Chem. Soc. 138 (2016) 1010.
[26] S. Zou, Y. Liu, J. Li, C. Liu, R. Feng, F. Jiang, et al., Stabilizing cesium lead halide perovskite lattice through Mn (II) substitution for air-stable light-emitting diodes, J. Am. Chem. Soc. 139 (2017) 11443.
[27] J. Klarbring, Low-energy paths for octahedral tilting in inorganic halide perovskites, Phys. Rev. B 99 (2019) 104105.
[28] J. Young, J.M. Rondinelli, Octahedral rotation preferences in perovskite iodides and bromides, J. Phys. Chem. Lett. 7 (2016) 918.
[29] L.D. Whalley, J.M. Skelton, J.M. Frost, A. Walsh, Phonon anharmonicity, lifetimes, and thermal transport in $CH_3NH_3PbI_3$ from many-body perturbation theory, Phys. Rev. B 94 (2016) 220301.
[30] F. Shojaei, W.-J. Yin, Stability Trend of Tilted Perovskites, J. Phys. Chem. C 122 (2018) 15214.
[31] W.J. Mir, A. Swarnkar, A. Nag, Postsynthesis Mn-doping in CsPbI3 nanocrystals to stabilize the black perovskite phase, Nanoscale 11 (2019) 4278.
[32] A. Pandey, S. Brovelli, R. Viswanatha, L. Li, J. Pietryga, V.I. Klimov, et al., Long-lived photoinduced magnetization in copper-doped ZnSe-CdSe core-shell nanocrystals, Nat. Nanotechnol. 7 (2012) 792.
[33] T. Telahun, U. Scherz, P. Thurian, R. Heitz, A. Hoffmann, I. Broser, Nonlinear Zeeman behavior of Cu^{2+} centers in ZnS and CdS explained by a Jahn-Teller effect, Phys. Rev. B 53 (1996) 1274.